Supplementary Information

Tuning the Branches and Composition of PtCu Nanodendrites through Underpotential Deposition of Cu towards Advanced Electrocatalytic Activity

Lin Guo,[abc] Lin-Bo Huang,[bd] Wen-Jie Jiang,[bd] Zi-Dong Wei,*[c] Li-Jun Wan[bd] and Jin-Song Hu*[bd]

[a] Key Laboratory of Photochemical Conversion and Optoelectronic Materials, Technical Institute of Physics and Chemistry, Chinese Academy of Sciences, Beijing 100190, China.

[b] Key Laboratory of Molecular Nanostructure and Nanotechnology, Institute of Chemistry, Chinese Academy of Science, Beijing, 100190, China; E-mail: hujs@iccas.ac.cn

[c] State Key Laboratory of Power Transmission Equipment & System Security and New Technology, College of Chemistry and Chemical Engineering, Chongqing University, Chongqing, 400044, China. E-mail: zdwei@iccas.ac.cn

[d] University of Chinese Academy of Science, Beijing 100049, China.

This file includes Experimental section and Figure S1-S11.

Experimental Section

Electrochemical measurements:

The cyclic voltammograms (CV) were carried out in Ar-purged 0.1 M $HClO_4$ solution at scan rate of 50 mV s^{-1}. The ORR polarization curves were recorded in O_2-saturated 0.1 M $HClO_4$ solution at a scan rate of 10 mV s^{-1} and a rotation speed of 1,600 rpm. The methanol oxidation reaction (MOR) were performed in Ar-purged 0.1 M $HClO_4$ + 1 M CH_3OH solution by potential cycling at a scan rate of 50 mV s^{-1} at room temperature. The loadings of all catalysts for all electrochemical measurements were fixed to ~22 μg_{Pt} cm^{-2}.

The electrochemical surface area (ECSA) of Pt in the catalysts was calculated using the Equation 1:

$$ECSA = \frac{[Q_H]}{0.21\ mC\ cm^{-2} \times [Pt]} \quad (1)$$

Where Q_H (mC) is the charge for the hydrogen adsorption/desorption of the CVs, 0.21 mC cm^{-2} is the electrical charge for monolayer adsorption of hydrogen on Pt surface, and [Pt] is the Pt loading on the working electrode.

The specific kinetic current densities (j_k) associated with the intrinsic activity of the catalysts can be obtained by the Equation 2:

$$j_k = \frac{j_d \times j}{j_d - j} \quad (2)$$

Where j is the measured current density, j_k is the kinetic current density, j_d is the diffusion-limited current density, respectively.

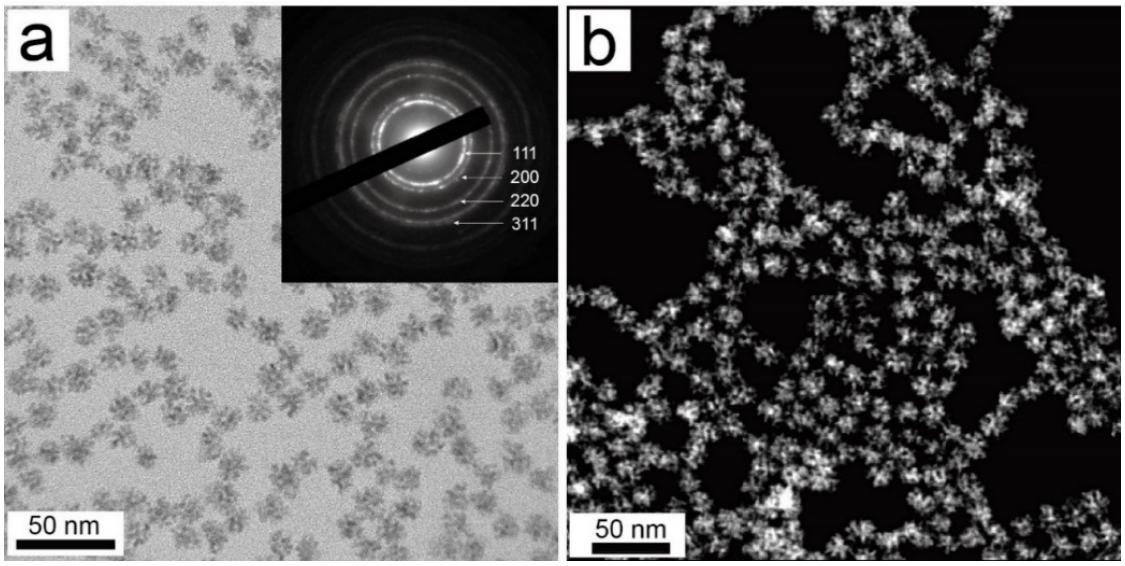

Fig. S1. a) low-magnification TEM image and b) HADDF-STEM image of $Pt_{55}Cu_{45}$ ND. The inset in Fig. S1a is the corresponding SAED pattern.

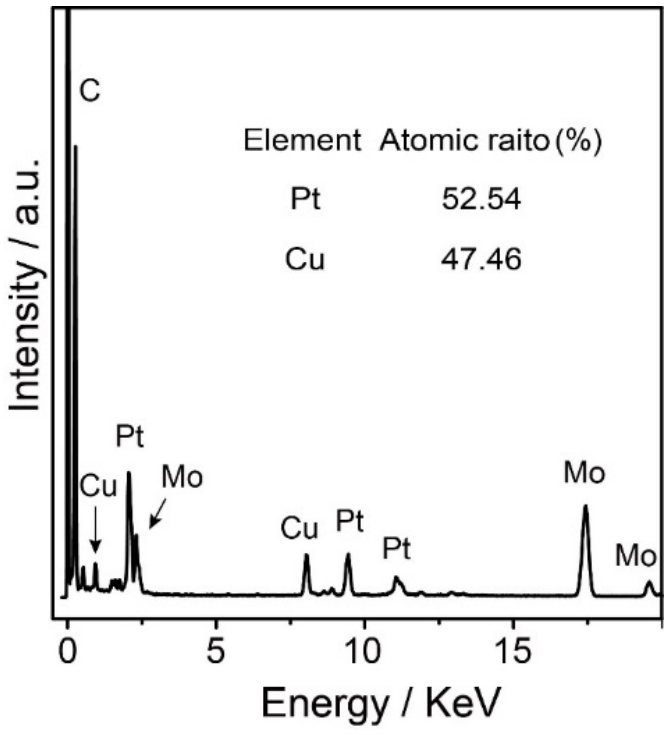

Fig. S2. EDS spectrum of $Pt_{55}Cu_{45}$ ND on a Mo-grid.

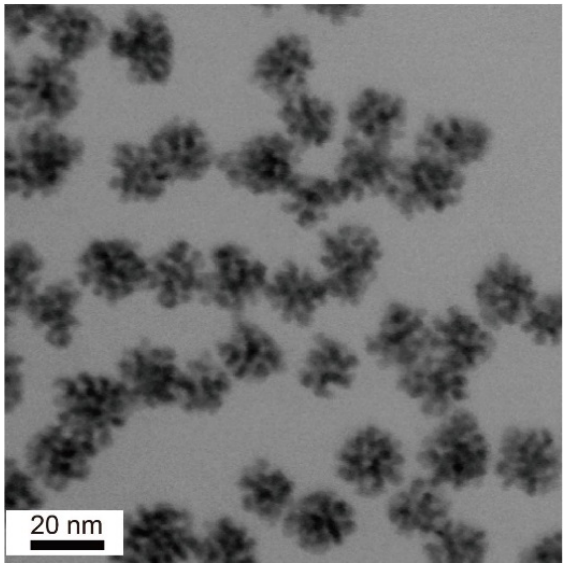

Fig. S3. STEM image of $Pt_{55}Cu_{45}$ ND

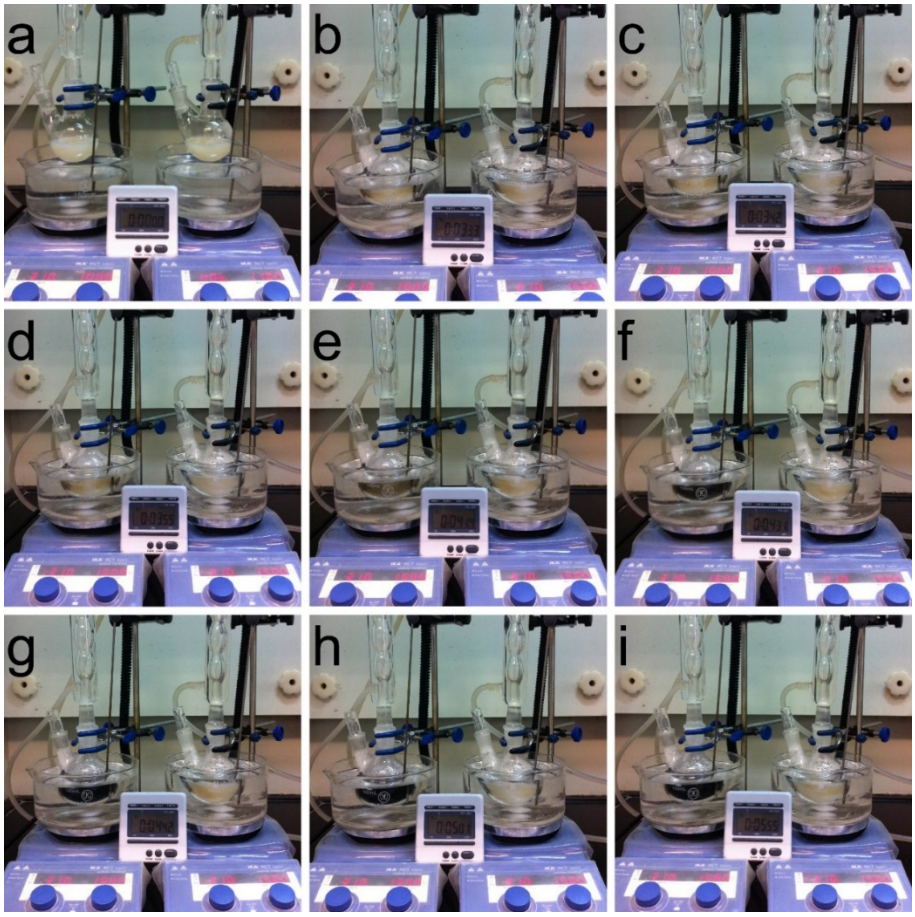

Fig. S4. Photos at different reaction timing during the synthesis of $Pt_{55}Cu_{45}$ ND (left) and Pt ND (right).

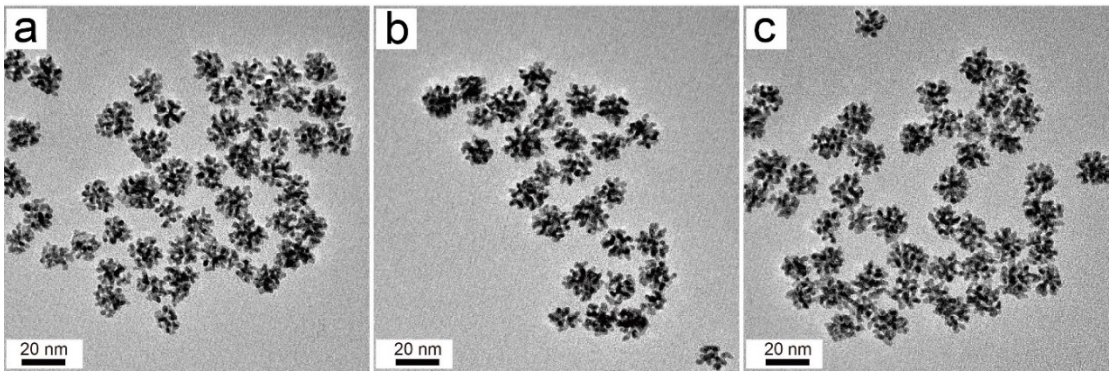

Fig. S5. TEM images of the products prepared with different Cu precursors: (a) $CuSO_4$, (b) $Cu(NO_3)_2$, and (c) $Cu(Ac)_2$.

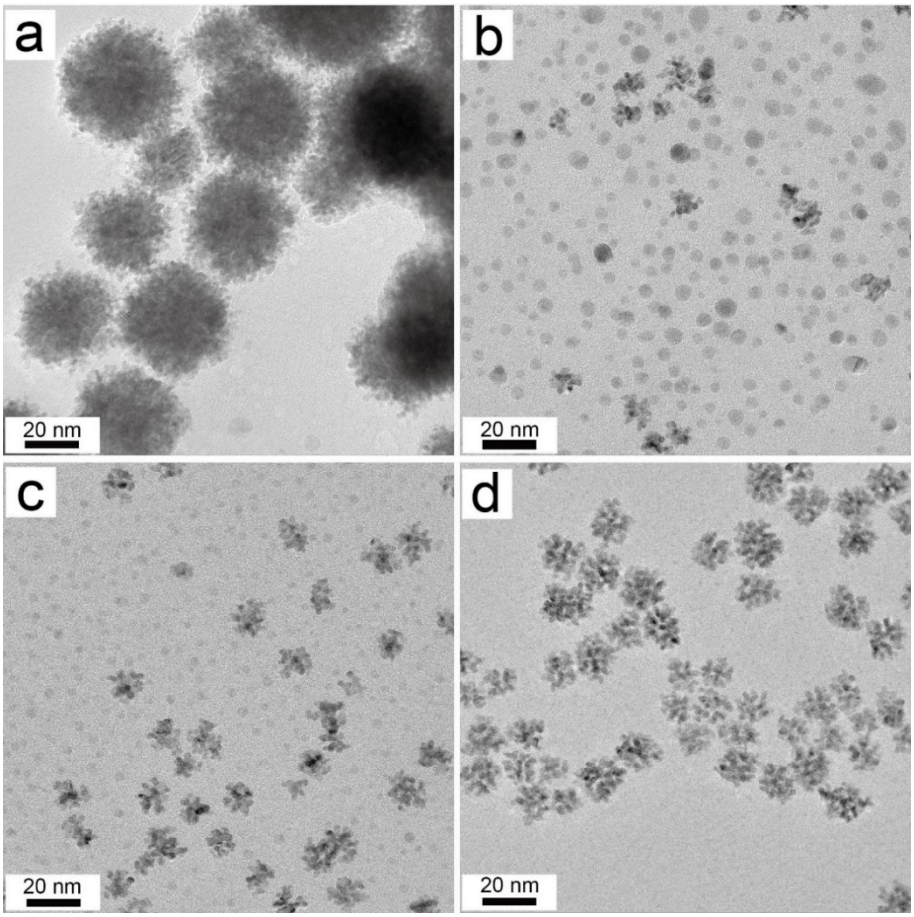

Fig. S6. Representative TEM images of the products obtained from the standard process except the different amount of CTAC: a) 0 mg, b) 10 mM, c) 15 mM, and d) 80 mM.

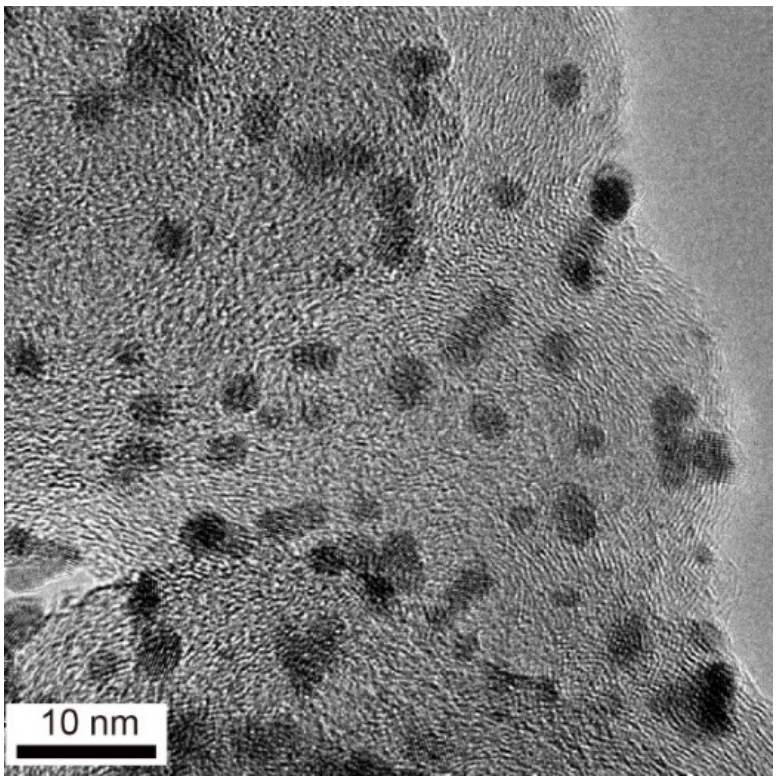

Fig. S7. Typical TEM image of JM Pt/C (20% Pt)

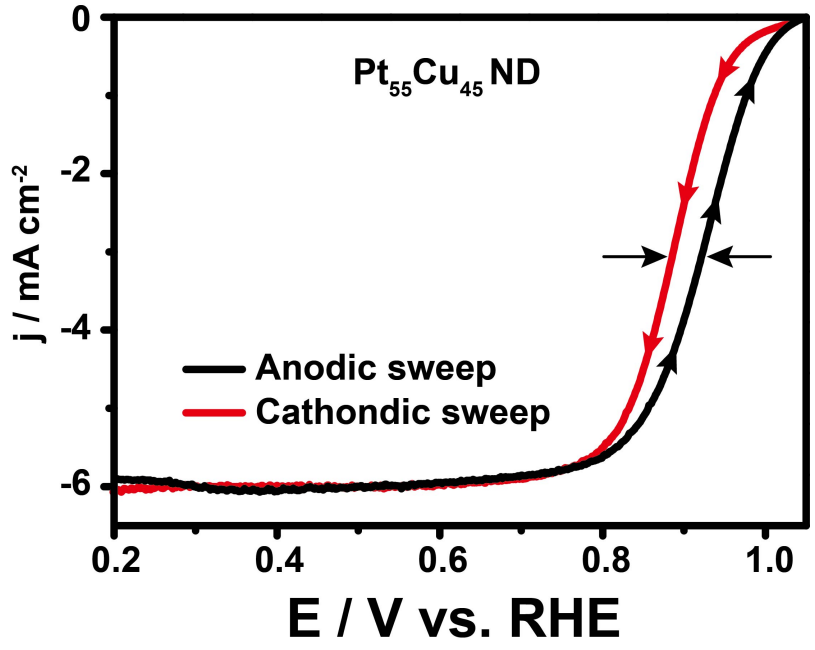

Fig. S8 ORR polarization curves for $Pt_{55}Cu_{45}$ ND recorded in an O_2-saturated 0.1 M $HClO_4$ solution at a sweep rate of 10 $mV \cdot s^{-1}$ and a rotation rate of 1600 rpm.

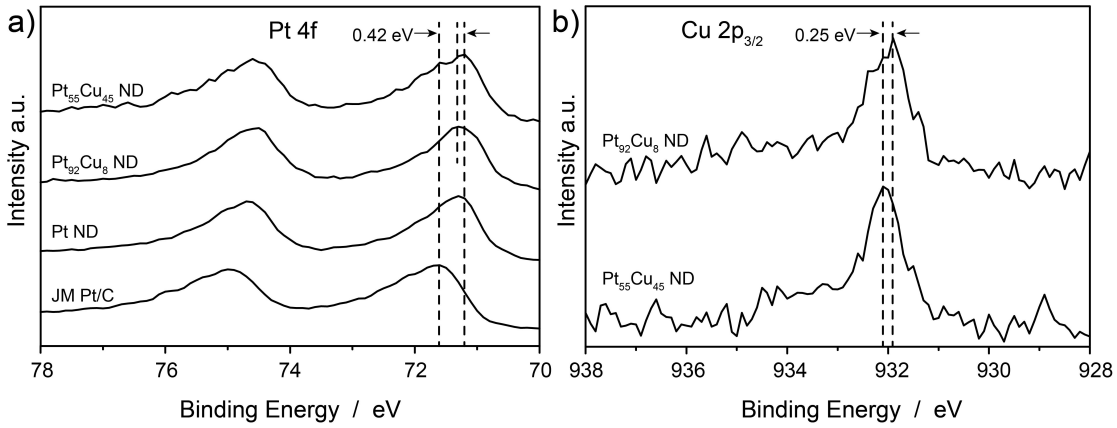

Fig. S9. a) Pt4f XPS spectra of $Pt_{55}Cu_{45}$ ND, $Pt_{92}Cu_{8}$ ND, Pt ND and JM Pt/C; b) Cu2p XPS spectra of $Pt_{55}Cu_{45}$ ND and $Pt_{92}Cu_{8}$ ND.

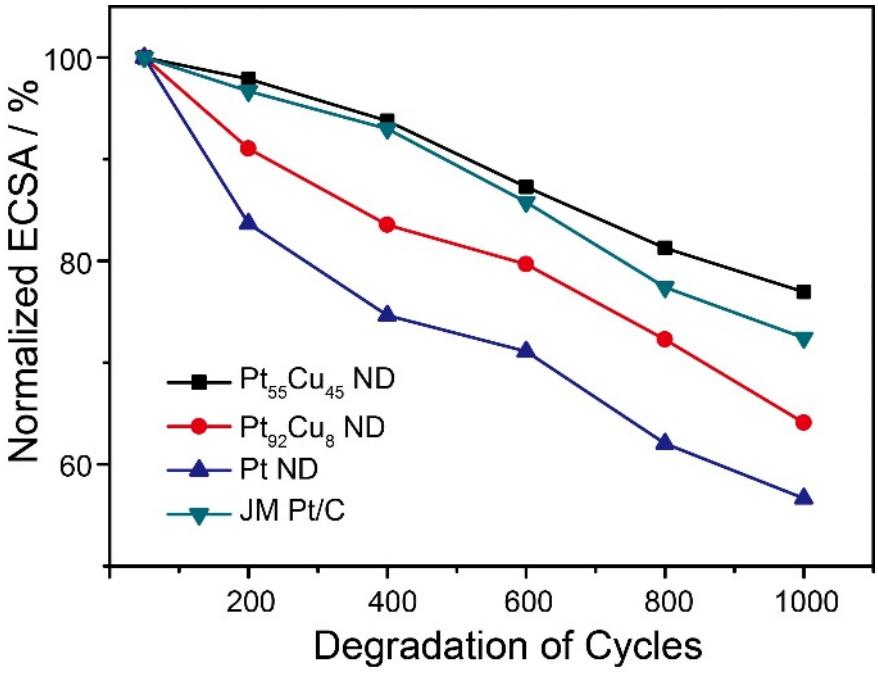

Fig. S10. ECSA loss of $Pt_{55}Cu_{45}$ ND, $Pt_{92}Cu_{8}$ ND, Pt ND and JM Pt/C with the increase of CV cycles.

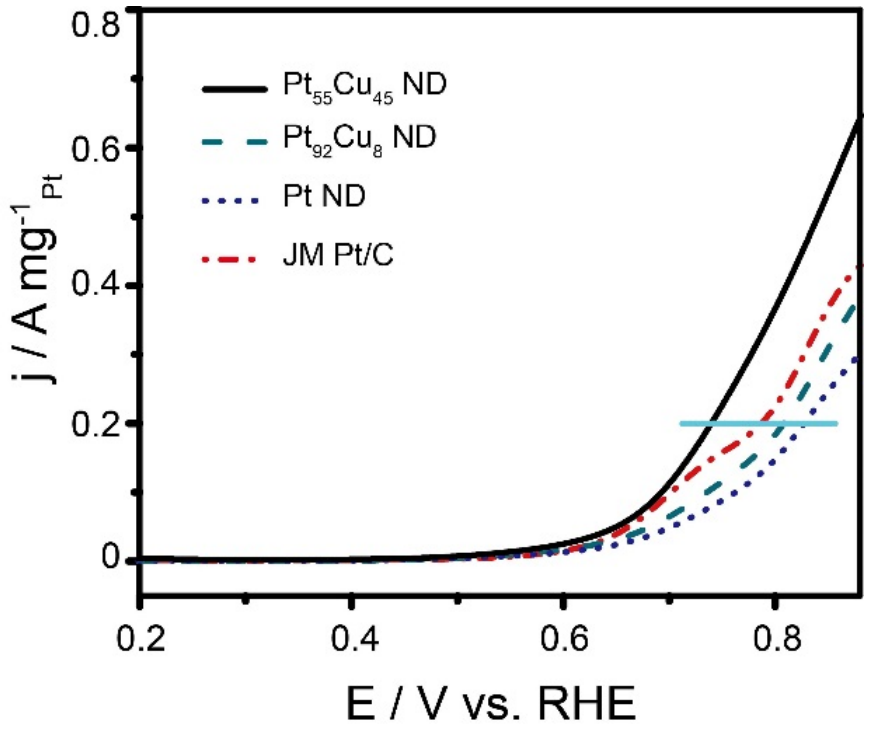

Fig. S11. Zoom-in LSV curves for MOR recorded in aqueous solution containing 0.1 M $HClO_4$ + 1M CH_3OH at a sweep rate of 10 $mV \cdot s^{-1}$, respectively.